

# An Investigation into Modeling Approaches for the Dynamic Response of a Shipping Container Cart and Suspended Automotive Parts Under Random Base Excitation using LS-DYNA®

Arun Ramanathan<sup>1</sup>, Scott Noll<sup>1</sup>, Eric DeHoff<sup>2</sup>, Ron Rittenhouse<sup>3</sup>

<sup>1</sup>The Ohio State University SIMCenter, Columbus, Ohio USA

<sup>2</sup>Honda R&D Americas, Raymond, Ohio USA

<sup>3</sup>Honda North America, Raymond, Ohio USA

## Abstract

Shipping containers are exposed to complex dynamic loading conditions during transport via truck, rail, and air. The loading conditions are further complicated by contact nonlinearities between the cart and ground, between cart holders and suspended parts, and between neighboring suspended parts. This study focuses on developing a modeling strategy to simulate a container cart with parts undergoing ASTM D4728 truck random vibration tests. Initially, the linear frequency-domain properties and response to a random excitation profile of the cart structure were examined and correlated with experimental measurements. The linear response predictions lacked the required modeling fidelity to capture the nonlinear dynamic behavior observed during the testing as the input power spectral density profile was increased to higher levels. Thus, the nonlinear response was then simulated in the time domain using the explicit integration method in LS-DYNA®. The use of LS-DYNA® also allowed the simulation of the complex contact-driven boundary conditions. The total run time was determined to be prohibitively long for the second approach as the time step size was 0.3 µsec for the required simulation duration of more than 5 sec. Finally, a dynamic substructuring strategy was employed through the use of super elements. This final approach captured the dynamic amplification of the cart, maintained the contact nonlinearities, and reduced the total run times. This modeling approach in LS-DYNA® appears promising to capture the complex dynamic loading conditions affecting shipping containers in a computationally efficient manner.

## 1 Introduction

The dynamic loading conditions for shipping containers during transport via truck, rail and air are complicated by several factors that can be classified as external, structural or by the vibratory signal. The external factors include the vehicle suspension, payload, platform location [1], vehicle speed [2], road surface conditions [3], and braking severity. The structural complexities include contact nonlinearities between the cart and ground, between cart holders and suspended parts, and between neighboring suspended parts. Transport-related vibratory signals are generally characterized as Gaussian and stationary in nature, as they enable one to conveniently study the phenomenon in the frequency domain by expressing the random vibration in terms of power spectral density and root mean square acceleration values. However, recent advances and emphasis on characterizing road vibrations to be non-Gaussian [4, 5] necessitates the system be modeled in the time domain.

Due to these complexities, packaging system designs are often evaluated through empirical means. Several studies [6-8] have examined vibration levels during truck transportation under various road conditions and the residual effect on the shipped goods. Experimental guidelines for shipping racks are established in ASTM D 4728 [9] and provide a uniform basis for evaluating shipping units in controlled laboratory conditions. Often, designs are modified on the basis of experience by increasing the strength of the shipped product or improving the shock absorption capacity of the packaging system. Thus, such processes depend on judgment and require iterative testing.

Prior studies have demonstrated the feasibility of using finite element models to evaluate the performance of packaging materials. For example, two recent studies [10-11] examined drop and impact test conditions for electronic devices. Such drop tests are short in duration, thus simulation times are manageable. Virtual manufacturing communities have shown interest in producing a set of

coordinated finite element models that are both high quality and fast enough to shorten the design cycle and decrease the cost [12-13]. Random vibration problems are typified by longer simulation times, and contact problems require finer mesh. Each makes the entire process computationally expensive, which reduces any design iterations and optimization studies on these models. To the best of the authors' knowledge, there is no prior published work that has undertaken nonlinear modeling of the random vibration of shipping containers.

To fill these voids, this article conducts an in-depth experimental and computational study of a selected shipping container. The study investigates both linear, random vibratory response and the feasibility of studying the nonlinear response to vertical random excitation with commercially available LS-DYNA<sup>®</sup> finite element software. The emphasis is placed on development of a computationally efficient finite element model by utilizing a dynamic substructuring technique that permits random vibration studies in both time and frequency domains.

## 2 Problem Formulation

The focus of this article is on a class of transportation carts where the components are unconstrained and held in place due to gravity. A photograph of such a system is illustrated in Fig. 1 where the transportation cart is supporting five automotive parts. The primary excitation is the base motion introduced to the system in the vertical direction. During operation and testing, the cart may lose contact with the ground surface, and the automotive part may come in and out of contact with the transportation cart as well as other automotive parts in close proximity. The chief objectives of this article were as follows:

- Conduct dynamic experimental studies of a transportation cart under random excitation;
- Construct and analyze a three-dimensional, linear, dynamic finite element model of the experimental studies;
- Construct an efficient three-dimensional, nonlinear, dynamic finite element model of the experimental studies; and to
- Compare the dynamic responses of the experiments with the finite element model predictions.

The excitations applied in these experiments are in accordance with road profiles described in ASTM D4728 and were conducted at three different amplitude levels as shown in Fig. 2. The finite element model of the entire system was developed using commercially-available nonlinear dynamic software (LS-DYNA<sup>®</sup>). The analyses include linear frequency domain as well as nonlinear time domain numerical integration solutions. The materials for each component are considered linear elastic, and the nonlinearity exists in the form of contact. The frequency range of interest was 0 to 150 Hz, corresponding to the typical excitation bandwidth experienced during truck transport. Further, the selected transportation container had the capacity to carry ten individual automotive components, with five along the top row and an additional five along the bottom row; however, this study was limited to the case where a single part is supported at the end of the top row, as this location experiences the greatest dynamic motion amplification.



Fig.1: Photograph of the subject shipping cart shown with five automotive parts on top row and an empty bottom row.

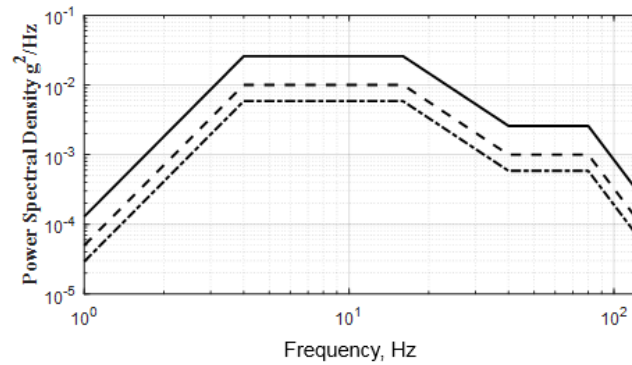


Fig.2: Power spectral density of the base excitation profiles in accordance with ASTM D4728. Key: (—) Level 1, (---) Level 2, (-·-·) Level 3.

### 3 Experimental Investigation

#### 3.1 Introduction

The experimental dynamic tests had two objectives: 1. to measure the modal properties of the cart structure in terms of natural frequencies, damping ratios, and mode shapes; and 2. to measure the motion transmissibility between the shaker floor to key observable locations on the cart structure. The modal measurements were conducted with three configurations: 1. shipping container only, 2. shipping container with one part, 3. shipping container with five parts. The shipping container was on a level concrete surface supported by the caster wheels. The system was excited and the responses were observed in the vertical direction. The test was conducted with a 512-Hz sampling frequency with a 1-Hz resolution. The sensitivity of the impact hammer and the accelerometer used was 2.2 mV/g and 100 mV/g, respectively. The frequency response functions were calculated using the  $H_1$  estimator and 5 averages with forced exponential decay applied to the output to avoid spectral leakage.

Configuration	Vibration mode description			
	Out-of-phase arm bending		In-phase arm bending	
	$\omega_1 / 2\pi$	$\zeta_1$	$\omega_2 / 2\pi$	$\zeta_2$
Shipping container only	21.8	1.76	26.5	0.96
Shipping container with one part	18.9	1.88	25.0	0.18
Shipping container with five parts	16.8	0.73	24.7	0.42

Table 1: Limited measured modal properties of the shipping container

The operational experimental schematic for conducting the ASTM 4728 random vibration tests is shown in Figure 3. The shipping container was placed on the rigid shaker table platform so that the applied base motion was uniform over the test surface. The shaker table produced a single direction of vertical motion as controlled levels of continuously variable amplitude throughout the desired range. The shipping cart was restricted in excessive in-plane motion with several fixtures and guides for safety purposes. Accelerometers were positioned to measure the response at each of the four caster wheels, the response at the arm tips, and the motion of the shaker table. The measurements from the accelerometers were taken at a bandwidth of 512 Hz for 50 seconds and 50 averages. Three levels of base excitation profiles were conducted in accordance with ASTM D4728.

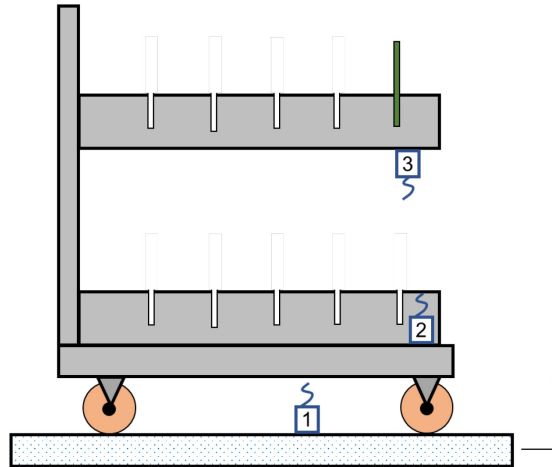


Fig.3: Schematic of the instrumentation for the ASTM D4728 experimental setup. Accelerometers located 1. at shaker base, 2. above caster wheel, and 3. at arm tip position.

### 3.2 Key Results

The tests were conducted under three configurations: 1. shipping container only, 2. shipping container with one part, and 3. shipping container with five parts. The power spectral density measured at the base (1), above a caster wheel (2), and at the arm tip (3) for the container only configuration at all three excitation levels is shown in Figure 4. No significant difference was observed between the measurements made by accelerometers placed at each caster wheel, as such, the measurement taken at a single location is considered as the representative of the measurements taken at all four caster wheels. Figure 4 illustrates the amplification of the base input excitation to the shipping container above the caster wheel and at the cantilevered arm tip at all excitation levels. Maximum amplifications of the power spectral density correspond to the natural frequencies of different arm modes observed in the modal tests (given in Table 1).

Figure 5 shows the effect of loading at various measurement points of the structure for the Level 3 excitation profile. The base and caster plate measurements were mostly unaffected by loading, whereas the arm tip exhibited greater sensitivity to the presence of the automotive part. The arm tip power spectral density was largely unaffected at frequencies below 20 Hz, the response decreased between 20 and 30 Hz, and the response generally increased above 30 Hz in comparison to the other observed locations on the shipping container. This sensitivity is attributed to the series of impacts due to bouncing of the part on the arm.

Table 2 summarizes the results from the random vibration test in terms of the overall acceleration level  $G_{rms}$ . An average amplification factor of 8.26 was observed between the base and the arm. It was observed that even though the peak acceleration levels were lowered when the shipping container as loaded, there was negligible change in the amplification factor obtained from these  $G_{rms}$  values.

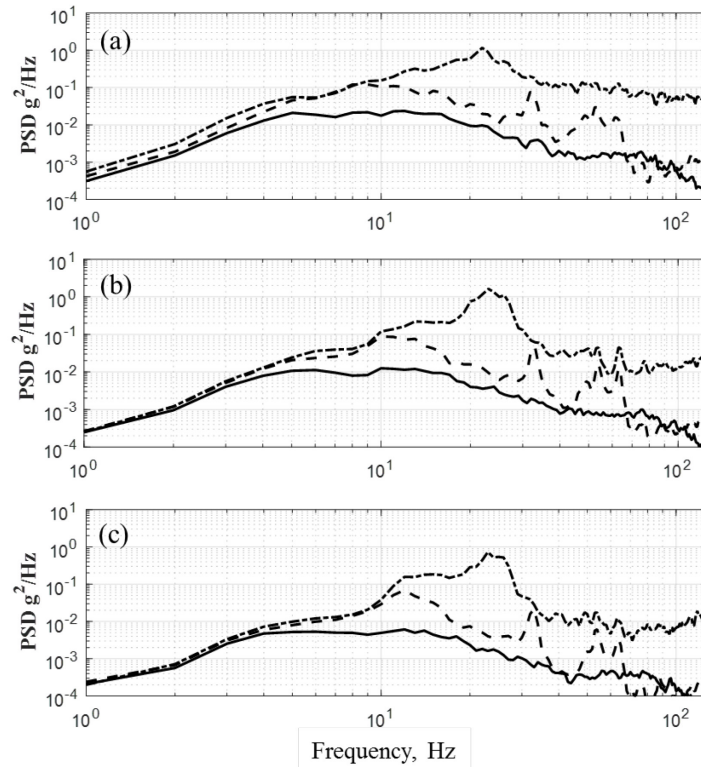


Fig.4: Acceleration power spectral density (PSD) measured for shipping container only configuration at (a) Level 1 excitation, (b) Level 2 excitation, (c) Level 3 excitation. Key: (—) shaker table base, (----) caster, (-·-·-) arm tip.

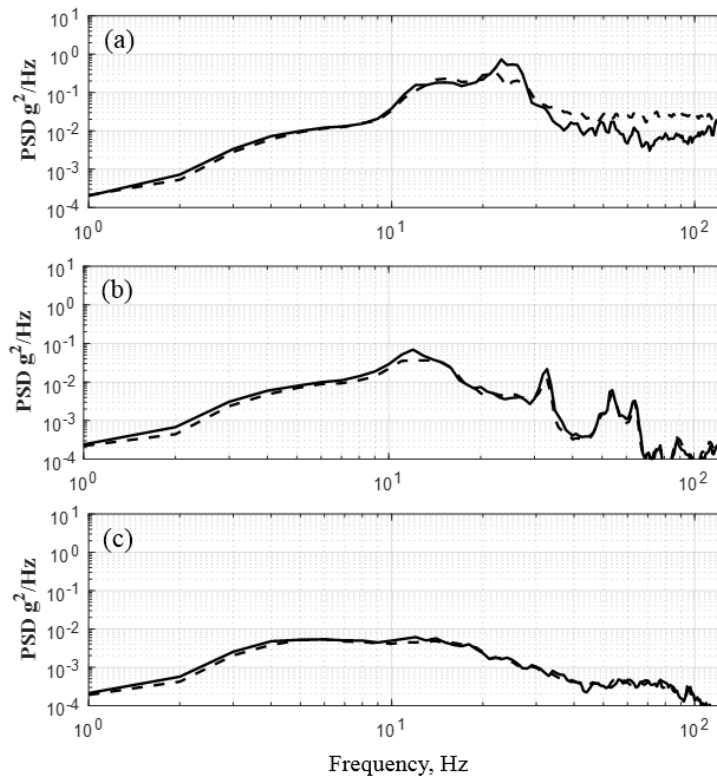


Fig.5: Effect of part loading under Level 3 excitation profile at (a) arm tip, (b) caster, (c) base. Key: (—) shipping container only, (----) shipping container with single part.

Configuration	Level	Location		
		Base	Caster	Arm
Shipping container only	1	0.7	1.71	6.71
	2	0.5	0.78	4.11
	3	0.35	1.23	2.72
Shipping container with one part	1	0.7	0.91	5.01
	2	0.49	1.35	4.08
	3	0.34	0.78	3.25

Table 2:  $G_{RMS}$  measured at key positions on the shipping container during the ASTM D 4728 tests.

#### 4 Finite Element Model

The finite element model of the transportation container included each component of the actual container with the exception of the caster wheel assembly. The structural components of the shipping container (shown in Fig. 6) are modeled with shell elements and assigned properties of cold rolled steel ASTM A366 with a Young's modulus of 210 GPa, density of 7850 kg-m<sup>-3</sup>, and a Poisson's ratio of 0.3. The automotive part holder is a plastic material with assumed properties for Young's modulus of 0.8 GPa, density of 970 kg-m<sup>-3</sup>, and a Poisson's ratio of 0.4. The shipping container system has approximately 700,000 degrees of freedom. The components of the shipping container assembly are connected via nodal rigid body elements. The boundary conditions are applied at the four caster plate locations using a pinned condition for the frequency step, and dynamic velocity excitations are imposed on the the identical nodes based upon measured data. The acceleration data measured at the rack caster wheels were post-processed to detrend signal drift due to noise and bias. Contact is established between the shipping container and the automotive parts using the penalty formulation. The parameters used for the contact formulation [14] are given in Table 3.

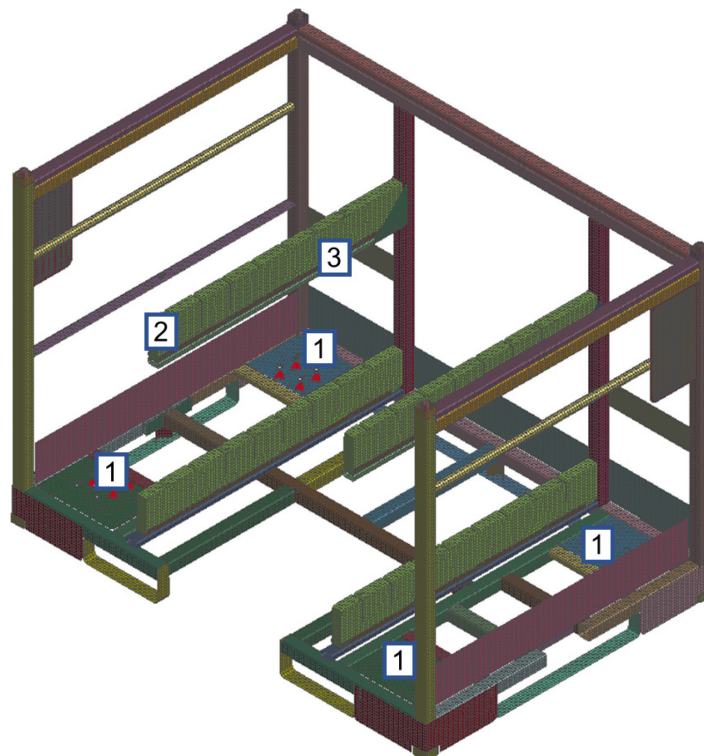


Fig.6: Finite element model of the shipping rack; 1. caster base, 2. arm tip, 3. arm holder.

Contact formulation	Soft constrained penalty formulation
Algorithm	Slave search contact algorithm
Static friction coefficient	0.3
Dynamic friction coefficient	0.2
Viscous damping coefficient	20%

Table 3: Contact model type and parameters at interface between the shipping container and automotive part.

## 5 Modal Parameter Correlation

An eigenvalue analysis of the finite element model was first performed using the Lanczos algorithm [15] within LS-DYNA, and the results were compared with the experiment. The measured modal properties allowed for an estimation of the modal damping ratios of the shipping container structure from which the Rayleigh damping coefficients,  $\alpha$  and  $\beta$ , were computed.

The frequency response function was synthesized within LS-Dyna using the mass normalized eigenvectors of the driving point and cross point. The first 100 modes that spanned from 0 Hz to more than 500 Hz were utilized, and the acceleration frequency response function was synthesized by the following expression:

$$|A_{ij}(\omega)| = \left| \sum_{r=1}^{100} \frac{-\omega^2 \{U_i\}_r \{U_j\}_r^T}{(\omega_r^2 - \omega^2) + j2\zeta_r \omega_r \omega} \right| \quad (1)$$

where  $A_{ij}(\omega)$  is the accelerance obtained when unit force is applied at  $i^{\text{th}}$  degree of freedom and acceleration is measured at  $j^{\text{th}}$  degree of freedom. Driving point accelerance is a special case with  $i=j$ . The comparison of the driving point accelerance with measurements in the Z-direction under the shipping container only configuration is shown in Figure 7. The modal damping ratio was calculated to be 2% from the measured frequency response function using the half-power bandwidth method. This equates to Rayleigh damping coefficients calculated with  $\omega = 27$  Hz to be  $\alpha = 0.22$  and  $\beta = 3.587 \times 10^{-4}$ .

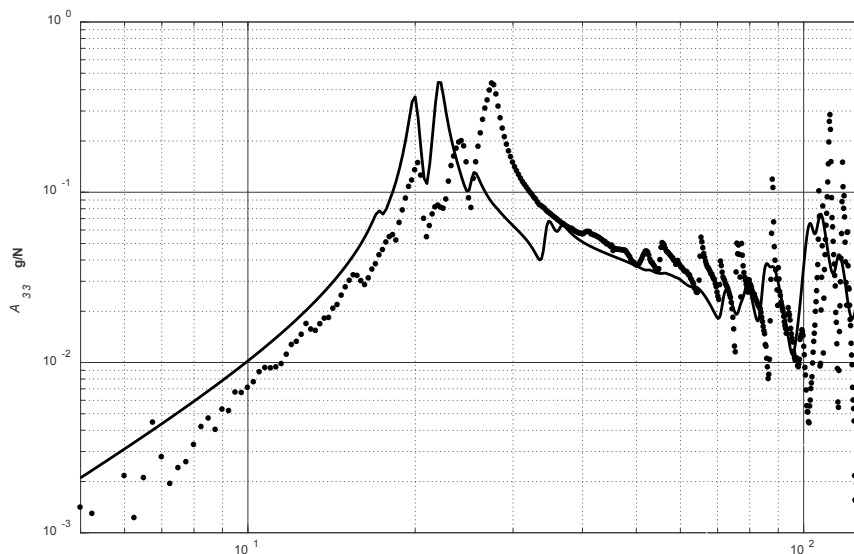


Fig.7: Comparison of measured and predicted driving point accelerance,  $A_{33}$ . Key: (—) complete finite element model, (●) measurements.

The peak response at the driving point frequency response function occurred at 22 Hz in the experiment compared to 27 Hz in the finite element model. The source of error between the measured and predicted response was likely that the actual shipping container was used and displayed significant wear and tear. The worn condition was not included in the finite element model.

## 6 Dynamic Substructuring

### 6.1 Component Model Reduction Techniques

There are a variety of methods proposed in the literature [16] to compute the reduction basis for large systems. The basic idea behind component model reduction methods in structural dynamics is in fact modal superposition, where the displacements are written in terms of normal modes and modal amplitudes.

$$\mathbf{u} = \sum_{j=1}^n U_j \eta_j \quad (2)$$

Applying this idea to a dynamic substructuring technique, some static modes are required in the reduction basis to represent the static deformation caused by external forces. The undamped equation of the motions of the substructure  $\mathbf{S}$  is given by

$$\mathbf{M}\ddot{\mathbf{u}} + \mathbf{K}\mathbf{u} = \mathbf{L} \quad (3)$$

The set of original degrees of freedom  $\mathbf{u}$  is transformed into a set of generalized degrees of freedom  $\mathbf{q}$ .

$$\mathbf{u} = \mathbf{R}\mathbf{q} \quad (4)$$

Here  $\mathbf{R}$  is the reduction basis of dimension  $n \times r$ , typically with  $r \ll n$ . Substituting (4) in (3),

$$\mathbf{M}\mathbf{R}\ddot{\mathbf{q}} + \mathbf{K}\mathbf{R}\mathbf{q} = \mathbf{L} + \boldsymbol{\varepsilon} \quad (5)$$

where  $\boldsymbol{\varepsilon}$  is the error, since the generalized degrees of freedom  $\mathbf{q}$  does not span the full solution set. Also, here the error is assumed to be only in the space not spanned by  $\mathbf{R}$ . Therefore, the orthogonality of  $\mathbf{R}$  with  $\boldsymbol{\varepsilon}$  yields  $\mathbf{R}^T \boldsymbol{\varepsilon} = 0$ . Using this property and pre-multiplying equation (5) by  $\mathbf{R}^T$ ,

$$\mathbf{R}^T \mathbf{M}\mathbf{R}\ddot{\mathbf{q}} + \mathbf{R}^T \mathbf{K}\mathbf{R}\mathbf{q} = \mathbf{R}^T \mathbf{L} \quad (6)$$

$$\tilde{\mathbf{M}}\ddot{\mathbf{q}} + \tilde{\mathbf{K}}\mathbf{q} = \tilde{\mathbf{L}} \quad (7)$$

where  $\tilde{\mathbf{M}} = \mathbf{R}^T \mathbf{M}\mathbf{R}$ ,  $\tilde{\mathbf{K}} = \mathbf{R}^T \mathbf{K}\mathbf{R}$ , and  $\tilde{\mathbf{L}} = \mathbf{R}^T \mathbf{L}$ .

Here the reduction basis  $\mathbf{R}$  can be any orthogonal set of Ritz vectors or approximate modes, which is computationally less expensive to compute than eigenvectors. The general algorithm to compute Ritz vectors is given in [17]. The various component reduction techniques differ from one another in the choice of this reduction basis  $\mathbf{R}$ . This work adopts the Craig-Bampton reduction technique, hence a brief overview of this technique is provided here.

### 6.2 Craig-Bampton Method

The Craig-Bampton method [18] forms the reduction basis  $\mathbf{R}$  by using two classes of modes, the constraint modes ( $\boldsymbol{\Psi}_c$ ) and the fixed vibration modes ( $\boldsymbol{\Phi}_{int}$ ). The constraint modes contain the static information, and the fixed vibration modes contain the internal vibrational information of the structure. The primary step involved in generation of the substructure is identifying the retained (boundary) degrees of freedom  $\mathbf{u}_b$  and eliminated (internal) degrees of freedom  $\mathbf{u}_i$ . The system equation in (3) is then partitioned as

$$\begin{bmatrix} \mathbf{M}_{bb} & \mathbf{M}_{bi} \\ \mathbf{M}_{ib} & \mathbf{M}_{ii} \end{bmatrix} \begin{Bmatrix} \ddot{\mathbf{u}}_b \\ \ddot{\mathbf{u}}_i \end{Bmatrix} + \begin{bmatrix} \mathbf{K}_{bb} & \mathbf{K}_{bi} \\ \mathbf{K}_{ib} & \mathbf{K}_{ii} \end{bmatrix} \begin{Bmatrix} \mathbf{u}_b \\ \mathbf{u}_i \end{Bmatrix} = \begin{Bmatrix} \mathbf{L} \\ 0 \end{Bmatrix}. \quad (8)$$

To include the vibrational information in a reduction basis, one must fix the boundary degrees of freedom, (i.e.) set  $\mathbf{u}_b = 0$ . This results in

$$\mathbf{M}_{ii}\ddot{\mathbf{u}}_i + \mathbf{K}_{ii}\mathbf{u}_i = 0 \quad (9)$$

This can be solved as an eigenvalue problem and results in a set of eigenfrequencies and eigenmodes  $\Phi_{\text{int}}$ .

The static information of the structure is then extracted by computing the constrained modes  $\Psi_c$ . This can be thought of as constructing equivalent stiffness matrix between the boundary degrees of freedom. The second equation in (8) is

$$\mathbf{M}_{ii}\ddot{\mathbf{u}}_i + \mathbf{M}_{ib}\ddot{\mathbf{u}}_b + \mathbf{K}_{ii}\mathbf{u}_i + \mathbf{K}_{ib}\mathbf{u}_b = 0. \quad (10)$$

Since it is considered a static problem, the inertial forces are zero, thus, equation (10) reduces to

$$\mathbf{K}_{ii}\mathbf{u}_i + \mathbf{K}_{ib}\mathbf{u}_b = 0 \quad \text{and} \quad (11)$$

$$\mathbf{u}_{i,\text{static}} = -\mathbf{K}_{ii}^{-1}\mathbf{K}_{ib}\mathbf{u}_b. \quad (12)$$

Now the original set of degrees of freedom  $\mathbf{u}$  is reduced to a set of boundary degrees of freedom ( $\mathbf{u}_b$ ) as

$$\begin{Bmatrix} \mathbf{u}_b \\ \mathbf{u}_i \end{Bmatrix} = \begin{bmatrix} \mathbf{I} \\ -\mathbf{K}_{ii}^{-1}\mathbf{K}_{ib} \end{bmatrix} \mathbf{u}_b = \Psi_c \mathbf{u}_b. \quad (13)$$

Since the original set of interface degrees of freedom ( $\mathbf{u}_b$ ) are retained, the primal assembly can be used to couple the substructure to other substructures or components of the remaining finite element model.

Using the internal vibrational information  $\Phi_{\text{int}}$  and constraint modes  $\Psi_c$ , the original set of degrees of freedom  $\mathbf{u}$  are written as

$$\{\mathbf{u}\} = \begin{Bmatrix} \mathbf{u}_b \\ \mathbf{u}_i \end{Bmatrix} = \begin{bmatrix} \mathbf{u}_b \\ \Psi_c \mathbf{u}_b + \Phi_{\text{int}} \boldsymbol{\eta}_i \end{bmatrix} = \begin{bmatrix} \mathbf{I} & 0 \\ \Psi_c & \Phi_{\text{int}} \end{bmatrix} \begin{Bmatrix} \mathbf{u}_b \\ \boldsymbol{\eta}_i \end{Bmatrix} = \mathbf{R} \begin{Bmatrix} \mathbf{u}_b \\ \boldsymbol{\eta}_i \end{Bmatrix}. \quad (14)$$

### 6.3 Development of the Shipping Container Substructure

The first step involves identification of linear and non-linear parts of the structure and substructuring the linear part. Fig 8a shows the parts of the shipping container rack that will be converted to a substructure, and Fig 8b shows the arm hanger that was retained for contact with the automotive parts.

The next step involves identifying the nodes, their corresponding degrees of freedom and the frequency range for the internal vibration modes of the substructure to retain. The nodes act as couplers to the complete model and preserve the physical framework of the substructure. Degrees of freedom are retained for excitation points through which energy enters the system. The excitation locations retained the vertical degree of freedom reflecting the excitation direction, whereas all six degrees of freedom were retained on the arm shown in Fig 8a.

Next, a frequency range is selected for the dynamic reduction. The internal vibration modes are retained up to 120 Hz. Using this approach, the 700,000 degrees of freedom model is reduced to a substructure with 34 static and 60 dynamic modes for a total of 94 degrees of freedom.

The substructure is assembled to the remaining portions of the finite element model by constraining the retained arm tip nodes to the underside of the arm hanger using nodal rigid body elements. Visually, the substructured models appear within the preprocessor, LS-PrePost, as shown in Fig 9.

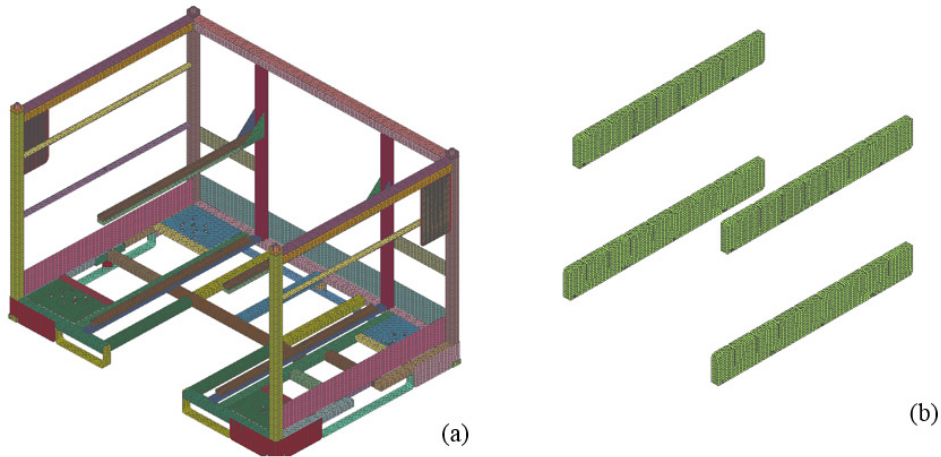


Fig.8: Partitioning of complete finite element (FE) model. (a) Substructured part of the FE model, (b) components retained in full.

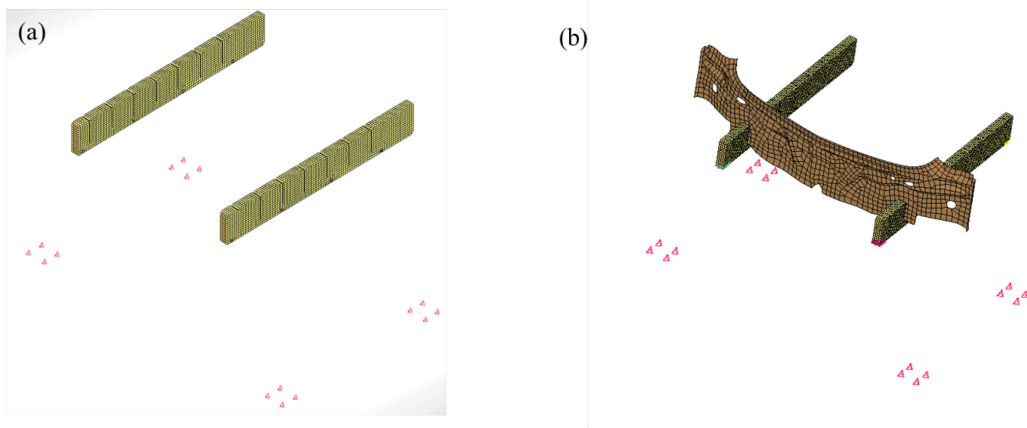


Fig.9: Finite element model with substructure. (a) Shipping container only configuration, (b) Shipping container with one-part configuration.

#### 6.4 Verification of the Dynamic Substructure Model

To prepare the dynamic substructure model for nonlinear random vibration simulations in the time domain, it is important to verify the linear characteristics of the substructured model with the complete finite element model. This can be done by comparing the driving point accelerance  $A_{33}$  of the substructured finite element model and the complete finite element model. It can be seen from Figure 10 that the substructured finite element model follows the complete finite element model up to 60 Hz as expected, and then the difference between them shows up. The accelerance can be made to comply further, beyond 60 Hz, by the addition of residual modes to the substructure [19] or by increasing the number of retained dynamic modes, but the current model does not necessitate the presence of modes beyond 60 Hz. With the verification process complete, these models can be used in the time domain simulation.

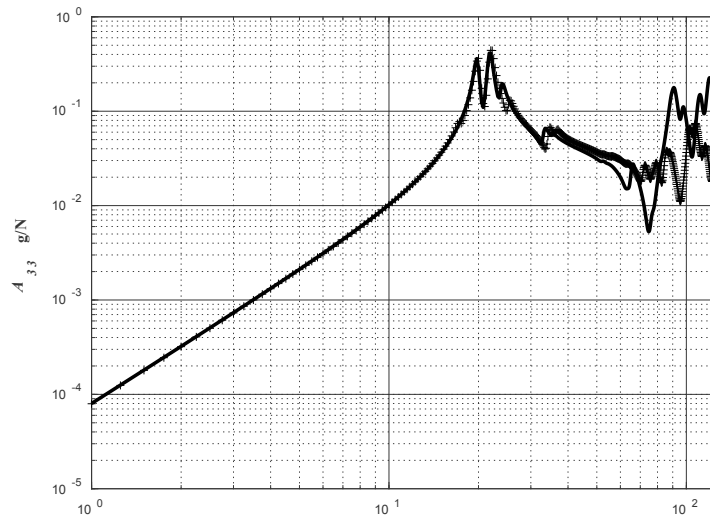


Fig.10: Comparison of the driving point frequency response function,  $A_{33}$ , for the substructured and complete finite element models. Key: (—) substructured finite element model, (+) complete finite element model.

### 6.5 Computational Time Comparisons

Fig. 11 shows the effect of various factors that were shown to influence computation time. All the cases shown here are simulations that are computed with an average mesh size of 20 mm (except for the case with finer mesh) for 1 s utilizing 64 processor cores. The following factors were found to affect computation time: 1. presence of substructure, 2. integration scheme, 3. mesh density, and 4. contact formulation. The figure is just an indicative and the identification of most computationally efficient model is very specific to the problem. If the model permits, addressing the random vibration problem entirely in the frequency domain using linearity assumptions is the most efficient way. For example, with the above configuration, the response power spectral density curve is computed in approximately 5 minutes; however, such an analysis is limited by the linearity assumption.

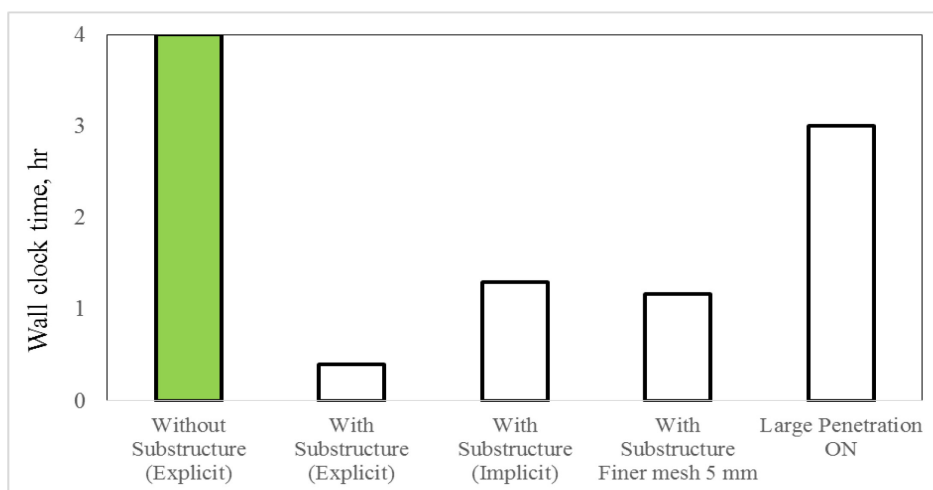


Fig.11: Effect of different factors on computation time. (■) Full model with penalty-based contact formulation, (□) substructured models.

## 7 Results

The substructured finite element model is subjected to the detrended vibratory input measured from directly above the caster wheel for a duration of 5 seconds with the simulation carried out with the explicit solver. Figure 12 shows the comparison of the power spectral density observed at the arm tip for both the simulations and measurements for the shipping container only configuration. There is good agreement up to 15 Hz; the results tend to diverge at and around 20 Hz. This difference between the model and experiment is attributed to the observations noted for the modal properties shown in Fig. 7. Here, the arm mode shapes differed between the experiment and model and have shifted the nonlinear dynamic amplification. Beyond 60 Hz, the response of the finite element model decreases. This difference in the response is attributed to an observation made during the experiments. Namely, several components of the actual shipping container exhibited clearance nonlinearities, and rattling was observed at the handle of the container, which was located far away from the arm tips. These clearances and subsequent rattles were not simulated in the current finite element model.

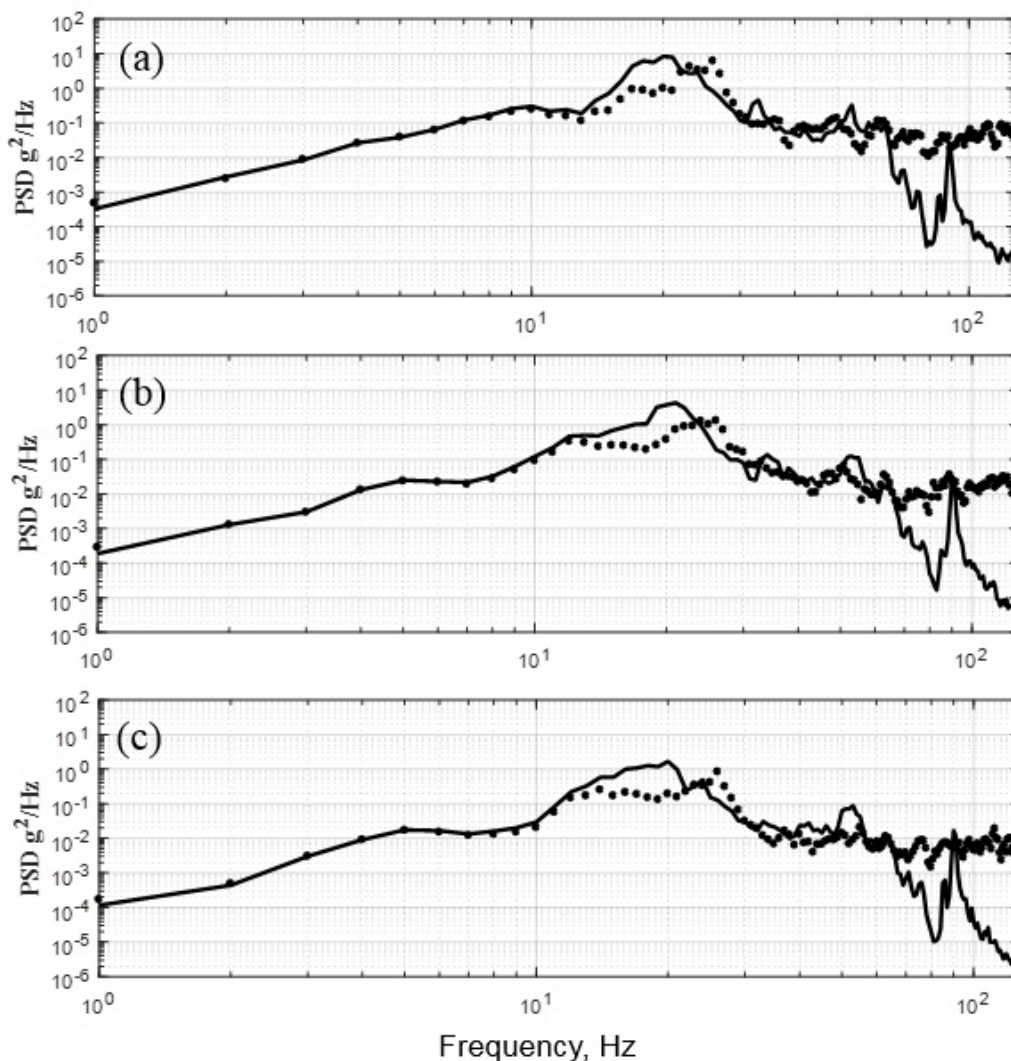


Fig. 12: Comparison of the measured and predicted power spectral density (PSD) at the arm tip for the shipping container only configuration, (a) Level 1 (b) Level 2 (c) Level 3 excitation. Key: (—) finite element model, (●) measurement.

Figure 13 shows the comparison of the power spectral density measured at the arm tip for both simulation and measurements for the one automotive part configuration. Here, the simulation includes

the clearance nonlinearity between the cart and part. Similar to the prior result, the results diverge in and around the arm modes.

Note that the magnitude of the response does not decrease significantly above 60 Hz as with the shipping container-only configuration (see Fig. 12). This supports the hypothesis that the unmodeled clearance and subsequent rattling explains the observed differences between the experiment and model. Such repeated impact events of the parts on the arm provide a broadband excitation and response.

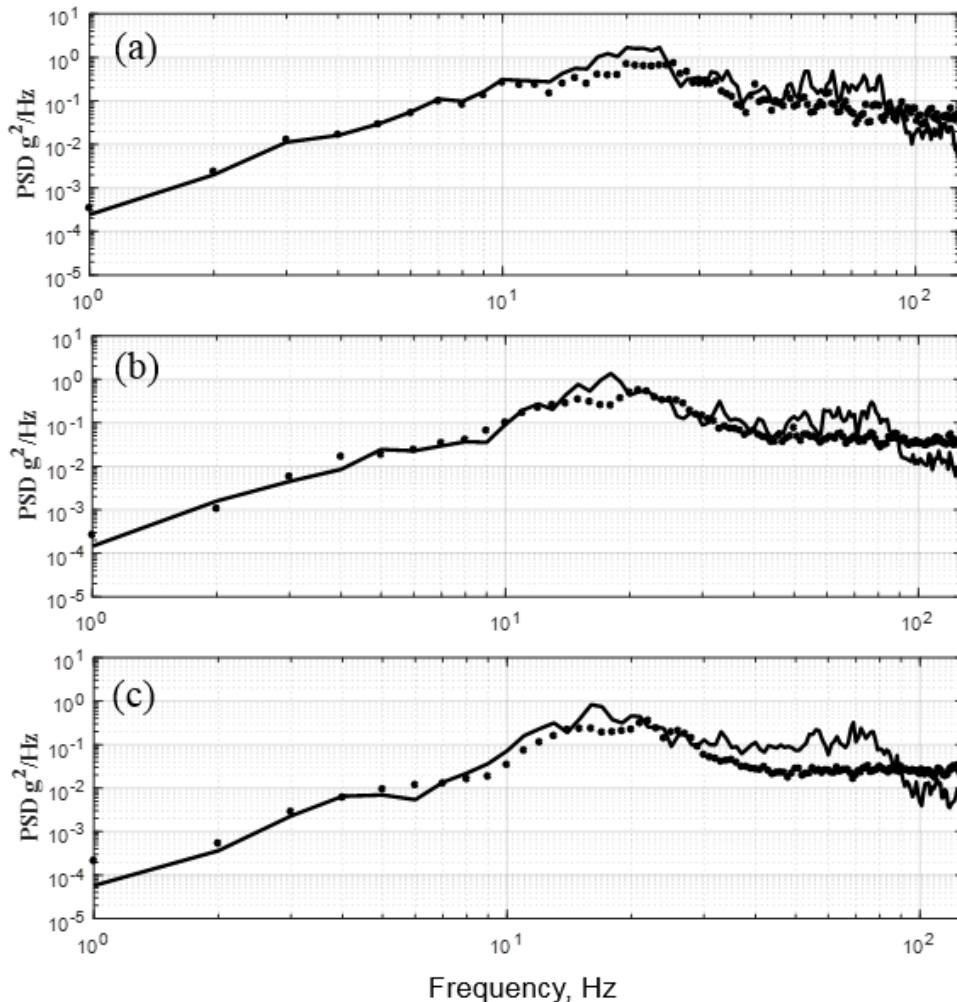


Fig.13: Comparison of the measured and predicted power spectral density (PSD) at the arm tip for the shipping container with one part configuration, (a) Level 1 (b) Level 2 (c) Level 3 input excitation. Key: (—) nonlinear finite element model, (●) measurement.

Motion transmissibility between the caster and the arm tip (see Fig. 14) was obtained from a linear finite element model and compared against the motion transmissibility from the measurements and the nonlinear finite element simulation. Comparing both the linear and nonlinear predictions provides an illustration of the significance of the nonlinearity present in the system as well as the extent to which linear system theories could be applied for further analysis. Generally, there is agreement between both models up to 20 Hz where the linear model prediction begins to deviate from the nonlinear model prediction and experiment. This result demonstrates that, for the subject system, linear frequency response functions provide some useful information on dominant arm modes of the system; however, linear theory does not have sufficient fidelity to capture the nonlinear dynamic behavior.

Table 4 shows the comparison of overall acceleration levels observed at the arm tip in both the configurations at all three input levels. There is no significant difference observed in the overall

acceleration levels when comparing the linear and nonlinear finite element models for the shipping container-only configuration, whereas the linear finite element model underpredicts the response in the case of the container with one part configuration. This is due to the absence of broadband excitation caused by the impact of the parts on the arm in the linear finite element model.

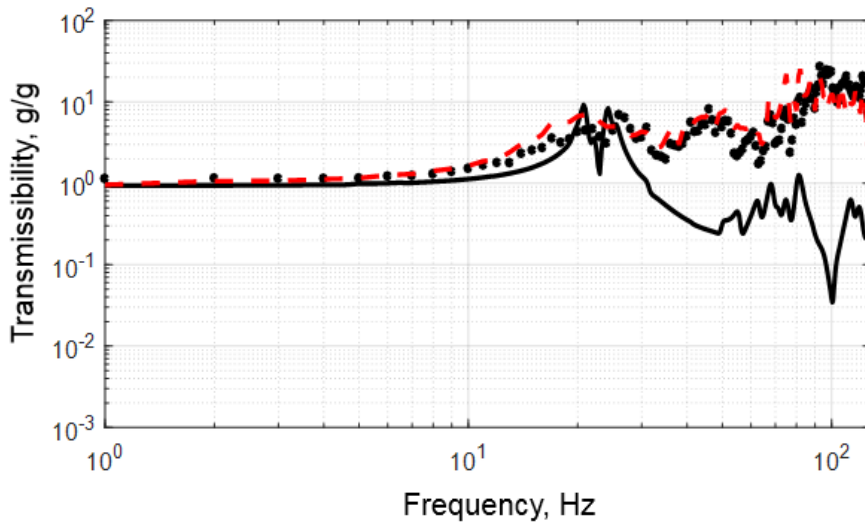


Fig.14: Comparison of motion transmissibility between the linear finite element model, the nonlinear finite element model and the experiment for the shipping container with one part configuration. Key: ( — ) linear finite element model, (o) measurements, (---) nonlinear finite element model.

Configuration	Level	Measurement	Nonlinear finite element model	Linear finite element model
Shipping container only	1	6.71	7.22	6.12
	2	4.11	5.02	4.23
	3	2.72	3.39	3.01
Shipping container with one part	1	5.01	5.66	4.03
	2	4.08	4.25	2.57
	3	3.25	3.78	1.81

Table 4: Comparison of arm tip G for each load configuration and excitation level.

## 8 Summary

Dynamic experimental studies were conducted under random excitation of the shipping container cart based on the ASTM D4728 test method. The acceleration time histories measured at three locations on the cart, namely the base, the caster and the tip of the arm, demonstrated dynamic amplification from the base vibrations to the holder arm tip at all levels of excitation and load configurations. An efficient three-dimensional finite element model of the experimental studies was developed using dynamic substructuring technique. The model simulates longer time periods at a reduced computation cost while maintaining reasonable accuracy. Discrepancies in the model necessitated the importance of expanding the study into the realms of interfacial damping characterization and contact modeling between the cart and the suspended parts to increase the fidelity of the current model and should be pursued in future studies. The model also illustrated the significance of non-linear time domain modeling of the random vibration problem as significant differences between the linear and non-linear motion transmissibility were evident. The finite element model consistently captures the nonlinear random vibration phenomenon and predicted the overall root mean square acceleration levels within 10-20% for three levels of excitation.

## 9 Literature

- [1] Singh SP, "Vibration levels in truck shipments as a function of suspension and preload", J. Test. Evaluation, 1992, 20(6) 466-469.
- [2] Lu F, Ishikawa Y, Kitazawa H, Satake T, "Effect of vehicle speed on shock and vibration levels in truck transport", Packaging Technology and Science 23 (2010) 101-109.
- [3] Jarimopas B, Singh SP, Saengni W, "Measurement and analysis of truck transport vibration levels and damage to packaged tangerines during transit". Packaging Technology and Science 2005; 18(4): 179-188.
- [4] Rouillard V, Lamb M, "On the effects of sampling parameters when surveying distribution vibrations", Packaging Technology and Science 2008; 21: 467-477.
- [5] Avendaño-Valencia LD, Fassois SD, "Stationary and non-stationary random vibration modelling and analysis for an operating wind turbine", Mechanical Systems and Signal Processing 47 (2014) 263-285.
- [6] S. P. Singh SP, G. J. Burgess GJ, P. Rojnuckarin P, "Test protocol for simulating truck and rail vibration and rail impacts in shipments of automotive engine racks", Packaging Technology and Science 8 (1995) 33-41.
- [7] Singh J, Singh SP, E Joneson, "Measurement and analysis of US truck vibration for leaf spring and air ride suspensions and development of tests to simulate these conditions", Packaging Technology and Science 19 (2006) 309-323.
- [8] Singh SP, "Measurement and analysis of US truck vibration levels on warehouse and retail store material handling and equipment", Journal of Applied Packaging Research 2 (2007).
- [9] "Standard Test Method for Random Vibration Testing of Shipping Containers", ASTM D4728 (2012).
- [10] Zhang C, Saito K, Kawaguchi K, Setoue H, "The hybrid drop test", Packaging Technology and Science 27 (2014) 509-520.
- [11] Wang YY, Lu C, Li J, Tan XM, Tse YC, "Simulation of drop/impact reliability for electronic devices", Journal of Finite Element Analysis and Design 41 (2005) 667-680.
- [12] Su H, "CAE virtual durability tests of automotive products in frequency domain", SAE International 2008-01-0240.
- [13] Larsen SE, "CAE – A strategy for a large scale virtual vehicle engineering factory", SAE International 2011-01-1065.
- [14] "LS DYNA Theory Manual", 2006.
- [15] Lanczos C, "An iteration method for the solution of the eigenvalue problem of linear differential and integral operators", Journal of NIST Standards 45 (1950) 255-282.
- [16] van der Valk PLC, "Model reduction and interface modeling in dynamic substructuring", MS Thesis, 2010.
- [17] Arnold RR, Citerly L, Chargin M, Galant D, "Application of Ritz vectors for dynamic analysis of large structures", Computers and Structures, Vol 21, (1985) 461-467.
- [18] M. C. C. Bampton MCC, R.R. Craig RR, "Coupling of substructures for dynamic analysis". AIAA Journal, 6(7) (1968) 1313-1319.
- [19] Rixen DJ, "Dual Craig-Bampton with enrichment to avoid spurious modes", Proceedings of IMAC-XXVII (2009)